

**VOLATILES IN HIGH TITANIUM BASALTS FROM THE MOON.** J. J. Barnes<sup>1,2\*</sup>, F. M. McCubbin<sup>1</sup>, J. W. Boyce<sup>1</sup>, A. N. Nguyen<sup>1,3</sup>, and S. Messenger<sup>1</sup>. <sup>1</sup>ARES, NASA JSC, Houston, TX. <sup>2</sup>School of Physical Sciences, The Open University, Milton Keynes, U.K. <sup>3</sup>JETS JACOBS, NASA JSC, Houston, TX. \*jessica.j.barnes@nasa.gov

**Introduction:** Chlorine is an unusual isotopic system, being essentially unfractionated ( $\delta^{37}\text{Cl} \sim 0 \text{ ‰}$ ) between bulk terrestrial samples and chondritic meteorites [e.g., 1-2] and yet showing large variations in lunar, martian, and vestan (HED) samples (from  $\sim -4$  to  $+81\%$ , [3-10]). Among lunar samples, the volatile-bearing mineral apatite ( $\text{Ca}_5(\text{PO}_4)_3[\text{F},\text{Cl},\text{OH}]$ ) has been studied for volatiles in K-, REE-, and P (KREEP), very high potassium (VHK), low-Ti and high-Ti basalts, as well as samples representing the lunar highlands [3-8]. These studies revealed a positive correlation between *in-situ*  $\delta^{37}\text{Cl}$  measurements and bulk incompatible trace elements (ITEs) and ratios [7-8]. Such trends were interpreted to originate from Cl isotopic fractionation during the degassing of metal chlorides during or shortly after the differentiation of the Moon via a magma ocean. In this study, we investigate the mineralogical and textural occurrence of phosphates, and the volatile inventories of a group of samples for which new-era volatile data have yet to be reported – the high-titanium, high-potassium mare basalts (typically,  $>2000$  ppm bulk  $\text{K}_2\text{O}$ ).

**Samples and Methods:** We studied thin sections of three high-Ti, high-K basalts (also referred to as Type A basalts) from the Apollo 11 mission (10017, 10024, 10049). These samples have bulk  $\text{K}_2\text{O}$  contents between  $\sim 0.28$  and  $0.33$  wt.%,  $\text{P}_2\text{O}_5$  contents from  $0.15$  to  $0.16$  wt.%, and  $\text{TiO}_2$  contents from  $10.6$  to  $12.6$  wt.% [11-12]. They represent a sampling of the end-members of the high-Ti, high-K basalt group, whilst also displaying variations in ITE abundances. The basalts have crystallization ages ranging from approximately  $3.5$  to  $3.7$  Ga [11 and references therein].

Thin sections were C coated and preliminary analyses and characterization work was conducted using the JEOL 7600F scanning electron microscope at JSC. Samples were initially X-ray mapped using energy dispersive spectroscopy (EDS) to locate P hotspots associated with the phosphates. Isotopic analyses of apatite in 10049 were conducted by isotope imaging on the JSC NanoSIMS 50L. The negative secondary ions of  $^{18}\text{O}$ ,  $^{19}\text{F}$ ,  $^{31}\text{P}$ ,  $^{35}\text{Cl}$ , and  $^{37}\text{Cl}$  were collected simultaneously with electron multipliers. A Cs+ primary beam of  $\sim 7$  pA was rastered over a range of areas ( $\sim 64$  to  $324 \mu\text{m}^2$ ). Well characterized apatite standards with a range of OH, Cl, and F contents and of known Cl isotopic compositions were used as primary reference standards

for calibrating both isotope ratios and volatile abundances.

**Phosphates in high-K basalts:** Apatite occurs as a late-stage mineral almost exclusively in mesostasis areas within the samples we investigated thus far. It typically coexists with plagioclase, high-Fe pyroxene, silica, ilmenite, troilite, K-rich residual glass, K-Ba feldspar, Zr-bearing minerals, and REE-merrillite. Apatite is present either as (i) discrete crystals varying from basal to acicular, most are euhedral with some being sub-hedral (Figure 1), and (ii) apatite-merrillite intergrowths. The intergrowths vary in texture from hexagonal crystals containing both phosphates typically within the mesostasis to vein-like merrillite with minor anhedral apatite, the latter are more commonly located at the boundary of, or cross-cutting through, the main rock-forming minerals (e.g. pyroxene). The observed intergrowth textures are strikingly similar to those reported in lunar highlands samples and KREEP-rich basalts [e.g., 13-14]. Apatite crystal size varies amongst the samples studied (which themselves vary from very fine to medium grained basalts) from  $<1 \mu\text{m}$  to  $\sim 60 \mu\text{m}$  in the longest dimension.

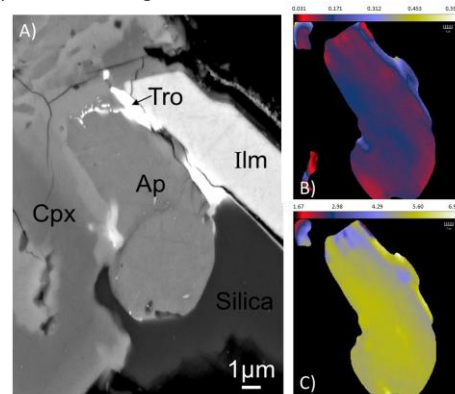


**Figure 1:** A) Backscattered electron image showing the petrographic setting of an apatite crystal in 10049. Tro = troilite, Cpx = clinopyroxene, Ap = apatite, and Ilm = ilmenite, B) Cl/P and C) F/P isotope ratio images. The color scale bars on the isotope images vary from low to high ratios from left to right (i.e., black to white).

**Results of the isotopic analyses of high-K, high-Ti basalt:** We used isotope imaging on the NanoSIMS to obtain the Cl isotopic composition [ $\delta^{37}\text{Cl} \text{ (‰)} = ((^{37}\text{Cl}/^{35}\text{Cl})_{\text{sample}} / (^{37}\text{Cl}/^{35}\text{Cl})_{\text{standard}}) - 1) \times 1000$ ] of five apatite crystals in 10049, which ranges from  $\sim -2.7 \pm 2 \text{ ‰}$  to  $+8.5 \pm 1 \text{ ‰}$  ( $2\sigma$ ). Using the volatile calibration determined by NanoSIMS analysis of apatite standards,

the F content of the apatite crystals analyzed in 10049 varied from 3.16 to 3.7 wt.% and the Cl content from 0.02 to 0.21 wt.%.

**Volatiles in high-Ti mare basalts:** Of the high-Ti basalts (>9 wt.% bulk TiO<sub>2</sub>) only members of the low-K sub-group have been investigated previously for  $\delta^{37}\text{Cl}_{\text{Ap}}$ : Apollo 11 samples 10044 and 10058, and Apollo 17 samples 70017, 70035, and 75055 [7-8,16] (Figure 2). In these samples apatite is most commonly fluorapatite, is usually located within late-stage mesostasis areas, and the samples are typically devoid of REE-merrillite. Of the mare basalts analyzed the high-Ti basalts show larger intra-sample H-isotope variations on the order of ~200 to 300 ‰ (2 SD) at relatively restricted OH contents when compared to low-Ti basalts [14-17]. In this volume, Barnes *et al.* [18] show that the same appears to be true for Cl-isotope compositions, with intra-sample variations on the order of 6 to 8 ‰ (2 SD), roughly double that observed for apatite in low-Ti mare basalts. Figure 2 shows the Cl-isotope compositions for apatite in lunar basalts compared with bulk rock Th abundances. In comparison to the high-Ti, low-K basalts, apatite from the most geochemically evolved [12] Apollo 11 high-K basalt (10049) show lighter  $\delta^{37}\text{Cl}$  values, whilst displaying Th abundances similar to those of KREEP basalt 72275 (i.e., ~135 × C.I. chondrite).

**Petrogenesis of the high-Ti basalts in light of Cl isotopes:** Simply following the models of [7-8] for lunar rocks with high bulk abundances of ITEs we might expect the high-Ti, high-K basalts to contain apatite characterized by heavily fractionated Cl isotope compositions, i.e., Cl obtained from mixing between unfractionated mantle Cl (~0‰) and the urKREEP reservoir (possibly fractionated to >+25‰, [19]). However, the data obtained for 10049 do not conform to either the early degassing or mixing models (Figure 2). Current petrogenetic models for the origin of the high-Ti, high-K basalts do not include urKREEP assimilation into the lunar magma ocean (LMO) cumulate sources. This is based on observations of (i) lower La/Sm ratios [12,20], (ii) relatively LREE-depleted profiles [12,20], and (iii) depleted initial Nd and Sr isotopic compositions [21] of the high-Ti, high-K basalts compared to KREEP. Neal and Taylor [20] suggested that source region heterogeneity rather than assimilation could explain the geochemical characteristics of the high-Ti mare basalts. In addition, the source regions for the high-Ti basalts may have been affected by metasomatism [22]. As Neal and Taylor [20] point out, if the hypothetical metasomatic agent was a KREEPy fluid, then that could explain the trend towards KREEP-like La vs K composition of Apollo 11 high-Ti, high-K basalts. Alternatively, assimilation of a

lithology less evolved (lower La/Sm ratio) than KREEP could also reproduce the geochemical trends exhibited by the high-Ti, high-K basalts [e.g., 12]. The new data that we present provides evidence for the existence of regions in the lunar interior that are REE-enriched and contain Cl that does not share isotopic affinities with lunar urKREEP.

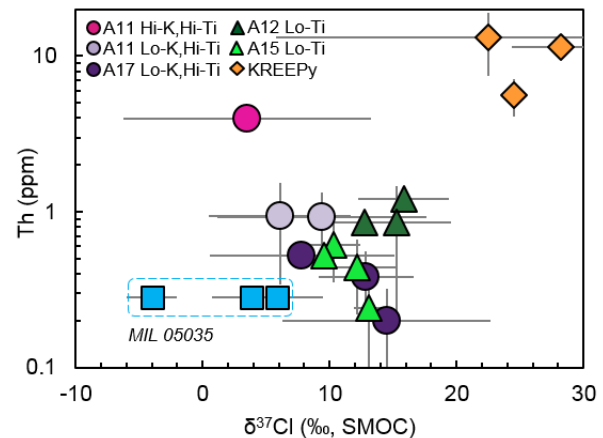


**Figure 2:** Average Cl-isotopic composition of apatite from Apollo lunar basalts [3-4,7-8,18] versus bulk rock Th abundances [11-12, additional references in 18]. The data points for low-Ti basaltic lunar meteorite MIL 05035 are the averages from multiple studies [4,7,18]. Uncertainties represent the standard deviation (2 SD) on reported values. SMOC refers to standard mean ocean chloride.

**Acknowledgements:** This work is supported by a NASA postdoctoral fellowship awarded to JJB and NASA's LASER program grant #NNX13AK32G awarded to F.M.M.

**References:** [1] Sharp Z. D. et al. (2007) *Nature* 446, 1062-1065. [2] Sharp Z. D. et al. (2013) *GCA* 107, 189-204. [3] Sharp Z. D. et al. (2010) *Science* 329, 1050-1053. [4] Wang Y. et al. (2012) *Proc. 75<sup>th</sup> Met. Soc.*, #5170. [5] Treiman A. H. et al. (2014) *Am. Mineral.*, 99, 1860-1870. [6] Tartèse R. et al. (2014) *Meteoritics & Planet. Sci.*, 49, 2266-2289. [7] Boyce J. W. et al. (2015) *Sci. Adv.*, 1, e1500380. [8] Barnes J. J. et al. (2016) *EPSL* 447, 84-94. [9] Williams J. T. et al. (2016) *MaPS* 51, 2092-2110. [10] Sarafian A. et al. (2016) *EPSL* 459, 311-319. [11] Meyer, C. (2012). Lunar Sample Compendium, and references therein. [12] Hallis L. J. et al. (2014) *GCA* 134, 289-316. [13] Elardo S. et al. (2012) *GCA* 87, 154-177. [14] Tartèse R. et al. (2014) *Geology* 42, 363-366. [15] Greenwood J. et al. (2011) *Nat. Geosci.*, 4, 79-82. [16] Barnes J. J. et al. (2013) *Chem. Geol.*, 337-338, 48-55. [17] Tartèse R. et al. (2013) *GCA* 122, 58-74. [18] Barnes J. J. et al. (2017) *Proc. XLVIII*, this volume #1724. [19] Boyce J. W. et al. (2017) *Proc. XLVIII*, this volume #1618. [20] Neal C. R. and Taylor L.A. (1992) *GCA* 56, 2177-2211. [21] Gaffney A. M. et al. (2007) *GCA* 71, 3656-3671. [22] Paces J. B. et al. (1991) *GCA* 55, 2025-2043.